RESEARCH ARTICLE

Speckle Reduction of PolSAR Images in Forest Regions Using Fast ICA Algorithm

Alireza Sharifi · Jalal Amini ·
Josaphat Tetuko Sri Sumantyo · Ryutaro Tateishi

Abstract Advancement in Polarimetric synthetic aperture radar technology (PolSAR) and its ability to capture images in different polarizations, facilitate accessing large volumes of information from a scene. These images as well as conventional SAR images are degraded by speckle noise. Processing and reducing the speckle of all the images separately is time consuming. So applying methods to simultaneously process different channels information can be very helpful. Several methods have been proposed for speckle reduction and each has advantages and disadvantages. In this paper, a despeckling approach based on fast independent component analysis (Fast ICA) algorithm is proposed for improving of the results when polarimetric channels are added. The results show the more input images to Fast ICA algorithm leads to better separation between signal components and the speckle. Analysis of the results for the ALOS (Advanced Land Observing Satellite) PALSAR polarimetric images showed that combination of polarimetric channels improved 37 % the ENL value in comparison with only using the HH (horizontal-horizontal)-, HV (horizontal-vertical)-, and VV (vertical-vertical)- polarized channels.

Keywords Independent component analysis · PolSAR · Speckle · Remote sensing

A. Sharifi
Department of Surveying and Geomatics Engineering, University of Tehran, Tehran, Iran 11155-4563
e-mail: alirezasharifi@ut.ac.ir

J. Amini (✉)
Department of Surveying and Geomatics Engineering, University of Tehran, Tehran, Iran 11155-4563
e-mail: jamini@ut.ac.ir

J. T. Sri Sumantyo
Center for Environmental Remote Sensing, Chiba University, Chiba 263-8522, Japan
e-mail: jtetukoss@faculty.chiba-u.jp

R. Tateishi
Center for Environmental Remote Sensing, Chiba University, Chiba 263-8522, Japan
e-mail: tateishi@faculty.chiba-u.jp

Introduction

Synthetic Aperture Radar (SAR) is an active remote sensing system typically mounted on a moving platform such as an aircraft or spacecraft. This system scores significantly compared to the other optical and infrared sensors because of some features such as ability to work in unfavorable weather conditions and in the night (Li et al. 2010). SAR polarimetry (PolSAR) has demonstrated, particularly during the last decade, its significance for the analysis and the characterization of the earth surface, as well as for the quantitative retrieval of biophysical and geophysical parameters. The capability to explore the complete space of polarization states represents one of the most important properties of PolSAR data, as optimization procedures may be foreseen. The second important property of PolSAR data is its inherent multidimensional nature that allows a more precise characterization of the scattering process at the resolution cell than single polarization data and, eventually, a better characterization of the scatter or scatters within that resolution cell (Gonzalez et al. 2012).

Regarding the interaction between incident electromagnetic waves and the target in both single and multi-polarization systems, the scattered power is determined by means of the scattering coefficient. Nevertheless, a polarimetric SAR has to be considered as a multi channel system. The images obtained from these systems are affected by an intrinsic factor called the speckle. This noise caused by the coherent interference of

recursive waves from several scatterings (Lee and Pottuier 2009; Li et al. 2010). The noise destroys texture and radiometric characterizations of SAR images and makes their interpretation difficult. Therefore, speckle filtering is a key preprocessing step for PolSAR images applications such as ship detection (Xinga et al. 2013), classification (Cheng et al. 2013; Dabboora et al. 2013), target decomposition (Zhanga et al. 2011), feature extraction (Kharbouchea and Claveta 2013), and biomass estimation (Amini and Sumantyo 2009).

Different methods have proposed to reduce speckles on single polarized SAR images that also can be suitable for filtering polarimetric images provided that they could be applied to the polarimetric covariance matrix elements. In general, SAR image filtering techniques can be divided to multi-look processing and post-processing filtering algorithms. In multi-look processing method, the synthetic aperture is divided into N parts and each part will create an image separately. The final image is obtained from the average images. This method decreases speckles variance, proportional with looks (N) but this is equal to proportionally loss of spatial resolution toward azimuth (Lee et al. 1991). Two of the early post-processing filters are mean and median filters. These filters are easily applied and remove a considerable amount of speckles, but they have two major drawbacks: The first, not considering the multiplicative property of speckle noise and the second, not being adaptive and applied equally to all parts of the image (Lee and Pottuier 2009). Therefore the tendency to use methods well adapted to the image is increased.

Adaptive filters are built based on the theory of Minimum Mean Square Error (MMSE). Such as Lee filter (Lee 1980), Kuan filter (Kuan et al. 1985), Frost filter (Frost et al. 1982), Gamma-MAP (Kuan et al. 1987), Enhanced-Lee and Enhanced-Frost (Lopes et al. 1990). Generally, these filters reduce the image speckle with local statistics and adjusting filter window. If the window size is large, the noise will be smooth and greatly reduced, but edges and point targets will have opacity of blurring, or conversely, if the window size is small and some of the edge information is maintained the speckle will not fit in properly. In recent years many methods have been developed to optimize the speckle reduction ratio with preserving edge detail and texture; two of these techniques are using wavelet transformation (Solbo and Eltoft 2002; Achim et al. 2003) and speckle reducing anisotropic diffusion (SRAD) (Yu and Acton 2002).

Methods exclusively exist for reducing noise of PolSAR images can be classified into two categories: The first set of methods filter all elements of the covariance matrix. These methods are very good for the physical and textural studies of ground targets in post-processing tasks and when the computation time is not important. But most of

these methods are powerless in simultaneous polarimetric processing of multiple channels and considering probable correlation between them. If using multiple channels, each channel should be processed independently and computation volume rises sharply. The second sets of methods only process the elements on main diameter of the covariance matrix. These methods apply for processing intensity images but in these methods polarimetric information will be lost. Among the latter, most methods only process one frequency band.

In recent years, independent component analysis (ICA) has been considered for reducing speckle and feature extraction in SAR images because of its good ability in separating blind sources (Lee and Hoppel 1992; Lopez-Martinez and Fabregas 2003; Ballatorea 2011; Chenab et al. 2011; Anticoa 2012). ICA separated statistical independent signals from linearly mixed signals. In this way, mixing model is detected with independent sources at the same time. Principal Component Analysis (PCA), as the basis and the infrastructure of ICA algorithm, was used much earlier than ICA in SAR images. Lee and Hoppel (1992) offered a PCA algorithm to reduce the speckle of PolSAR images that maximized signal-to-noise ratio. The high speed and accuracy of the ICA algorithm can be useful for many applications of PolSAR images such as biomass estimation, target detection and change detection.

Materials and Methods

Study Area

The study area is located in the north of Iran and south of Caspian Sea between 36°–36.5°N and 52° –52.5°E (Fig. 1). The natural vegetation of Sisangan forest is temperate deciduous broadleaved forest that is considered as one of the rainiest areas in Iran which is a suitable habitat for the broadleaf species. Figure 1 shows the coordinates of this area in the ETM-Landsat image that acquired in 4 December 2002 and related ALOS PALSAR data in three polarization channels that acquired in 22 May 2009.

Speckle Statistical Model in PolSAR Data

In this study, ALOS PALSAR data are analyzed which it was acquired during the dry season (to minimize any influence of varying rainfall and soil moisture) in 22 May 2009. The incidence angle and pixel spacing of this image are 30 m and 23.1°, respectively. Multipolarization SAR images are composed of four types of polarimetric images represented by scattering matrices. For each polarimetric channel, the statistics is like a single polarized image (Gao 2010). Therefore, studying

Fig. 1 ETM-Landsat image of study area acquired in 4 December 2002 (*upper panel*), and ALOS PALSAR Intensity images in HH-, HV, and VV-polarized channels that acquired in 22 May 2009 (*lower panel*)

L-HH   L-HV   L-VV
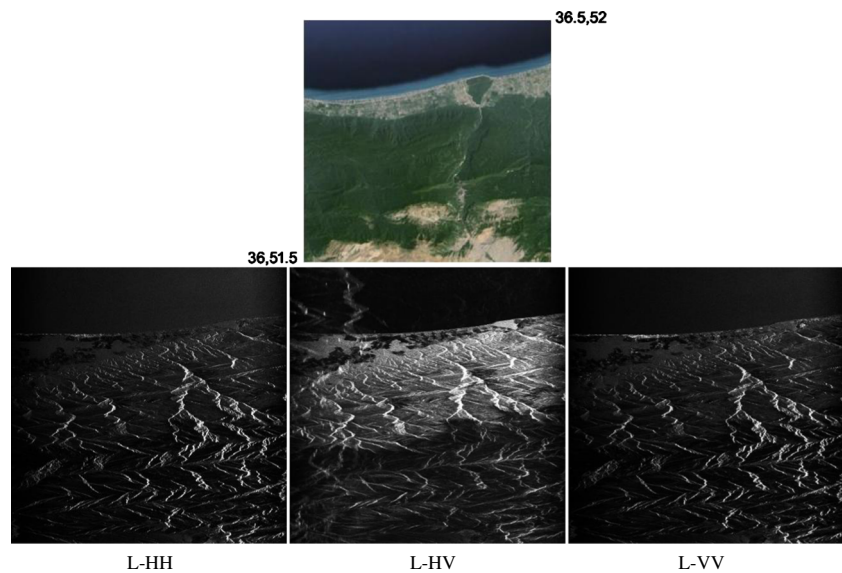
statistical model of single polarized SAR can be extended to describe more polarized channel. To define statistical models of a SAR image, different levels (in term of scattering) are divided into homogeneous, heterogeneous and highly homogeneous groups. Homogeneous group refers to an environment with moderate or poor backscattering. For example, smooth surfaces, slack water, and road have poor backscattering. Also, crops and rough surfaces have medium backscattering. Heterogeneous environment refers to targets like forests. Highly heterogeneous environment is known with strong backscattering as man-made objects, urban areas and steep slopes of the terrain.

Synthetic aperture radar acquires the backscatters from the target as amplitude and phase. Full polarimetric SAR data has scattering matrix for each sample as follow (Lopez-Martinez and Fabregas 2003):

$$S = \begin{bmatrix} S_{HH} & S_{HV} \\ S_{VH} & S_{VV} \end{bmatrix} \tag{1}$$

Where S_{HH} represents the scattering of transmitted wave with horizontal polarization and receiving it with the same polarization. The other three elements of the matrix are defined the same and the difference is only V, the symbol of vertical polarization. For the bilateral scattering and adjusted radar S_{HV} is equal to S_{VH}.

This format is suitable for single-look complex (SLC) data, but for multi-look complex (MLC) data it is better to use the covariance matrix to show the backscattering signal. In order to obtain the covariance matrix, polarimetric scattering data can be expressed by a complex vector:

$$k_1 = \begin{bmatrix} S_{HH} & \sqrt{2}S_{HV} & S_{VV} \end{bmatrix}^{\mathrm{T}} \tag{2}$$

Where T is the transpose sign and $\sqrt{2}$ has been used to maintain stability in the calculation of total power or Span:

$$Span(S) = |S_{HH}|^2 + 2|S_{HV}|^2 + |S_{VV}|^2 \tag{3}$$

The covariance matrix can be written as follows:

$$C = \langle k_l . k_l^T \rangle = \begin{bmatrix} \langle |S_{HH}|^2 \rangle & \sqrt{2}\langle S_{HH}S_{HV} \rangle & \langle S_{HH}S_{VV} \rangle \\ \sqrt{2}\langle S_{HV}S_{HH} \rangle & 2\langle |S_{HV}|^2 \rangle & \sqrt{2}\langle S_{HV}S_{VV} \rangle \\ \langle S_{VV}S_{HH} \rangle & \sqrt{2}\langle S_{VV}S_{HV} \rangle & \langle |S_{VV}|^2 \rangle \end{bmatrix} \tag{4}$$

Where asterisk (*) indicates the complex conjugate. As it can be seen, the sum of the main diagonal elements constitutes the total power and each main diagonal element is singly the intensity image of related polarimetric channel.

In the intensity images, speckle is multiplicative with original signal (Lee and Pottuier 2009). Assuming that the speckle has unique mean and is independent from signal, the multiplicative model can be rewritten as follows (Chitroub and Hachemi 2007):

$$x_i = s_i + s_i (n_i - 1) \tag{5}$$

Where x_i is the content of the pixel in the ith SAR image, s_i is noise-free signal response of target, and n_i is the speckle.

Some studies have used the logarithmic function to convert the multiplicative model to additive model and using the desired algorithm (Yusheng et al. 2005; Wang et al. 2008). The main drawback in applying this technique is that the dynamic range of the original image is compressed by the logarithm operation (Lee and Hoppel 1992).

Independent Component Analysis (ICA)

ICA is a statistical method for transporting observed multi-dimensional random vector to the mutually independent components. Compared with other methods based on second-order statistics, ICA not only can eliminate the first and second order correlation, but also can remove the high-order correlation data to obtain the independent components (Wang et al. 2008). ICA is a linear model as follows:

$$x = As = \sum_{i=1}^{n} s_i a_i \qquad (6)$$

Where x is the observed signal, A is mixer matrix, s is the independent component signal, and a_i is the ICA basis vectors. This model shows how the source signals provide observed signals. For estimating the A and s from the x, separator function is required (Eq. 7) to apply to the linear transformation, x, and source independent components, s.

$$y = Wx = WAs = W \sum_{i=1}^{n} s_i a_i \qquad (7)$$

Where W is separator function, and y is an estimation of s. In order to use this model, there are a number of constraints and assumptions: The first, initiatives of sources should be statistically independent. The second, at most one component should have a Gaussian distribution. For cases where more than one component is Gaussian, ICA can only separate non-Gaussian components but not Gaussian components. The third, the number of observed signal should be greater than or equal to the number of independent sources. If this condition is not met, the A matrix will not be reversible and s cannot be estimated (Yusheng et al. 2005; Wang et al. 2008; Wang 2009).

The Proposed Algorithm

In this study, the Fast ICA algorithm is used for despeckling of PolSAR images. Its advantage over other algorithms is in convergence speed and independency of user defined parameters. The steps of this algorithm are as follows (Wang 2009):

1. Pre-processing function, which is consists of centralizing, and whitening the observed signal and initializing W as a random vector.
2. Using the following replication equation to optimize W:

$$W_{k+1} = E\left\{ zg\left(W_k^T z\right) \right\} - E\left\{ g'\left(W_k^T z\right) \right\} W_k \qquad (8)$$

Where z is the whitened signal, g is nonlinear function and the g' is the derivative of the g function. Here we use $g=t^3$ as function.

3. Orthogonalization of W by symmetric orthogonal method.
4. Normalization of W: $\frac{W}{\|W\|} \rightarrow W$.

5. Make decisions based on whether or not W is convergent. If convergence is not created then it returns to step two.

In (Arsenault and April 1976) has shown that if the look is big enough ($L > 3$), the speckle remains independent of scene properties after additive logarithmic transformation. The goal is to prove the point that with increasing the number of input images, the noise of all the speckles are going to be Gaussian and we can use the ICA algorithm for better separating of signal from speckle. Concerning the proposed properties of ICA, this algorithm is capable of separating a Gaussian component from the other non-Gaussian components. Theoretically, increasing the number of inputs of an ICA algorithm, on one hand, the characteristics of the target signal rises and further details the target are available and on the other hand, the number of speckle samples increase. Since the noise samples are randomly distributed, according to central limit theorem, by increasing samples their distribution goes to Gaussian form. According to this theorem, the sums of random variables than any of them are more willing to go to the Gaussian distribution. So we can say that increasing the input data batch, the total noise signals are more likely to be Gaussian. In this way, the ability of ICA to separate the speckle set from target signal will increase.

If the noise random variable is n and the equivalent look is L, the probability density function will be as follows:

$$P(n) = \frac{n^{L-1} L^L}{\Gamma(L)} \exp(-nL) \qquad (9)$$

Where L is the shape parameter of the gamma distribution. If the image was single look ($L = 1$), the equation becomes the exponential distribution with unit mean.

Kurtosis is a criterion for understanding of distribution type:

$$Kurt(x) = \frac{E\left[(x-\mu)^4\right]}{\left(E\left[(x-\mu)^2\right]\right)^2} = \frac{\mu_4}{\sigma^4} \qquad (10)$$

Where μ and σ are mean and standard deviation of the random variable x, respectively. If the distribution of x is Gaussian, its kurtosis value will be three. If kurtosis is greater than three, the Gaussian probability density function of x is called the supper-Gaussian and if smaller than three it is called sub-Gaussian. Kurtosis of gamma function is as follow:

$$Kurt\,(gamma) = 3 + \frac{6}{L} \qquad (11)$$

Since the kurtosis of Gaussian function is 3, it is determined that the probability density function of speckle is supper Gaussian. The gamma distribution for large values of shape parameter (L) will converge to the Gaussian distribution. If the number of equivalent looks (L) increases, we can say that kurtosis value is approaching 3 (it goes to be
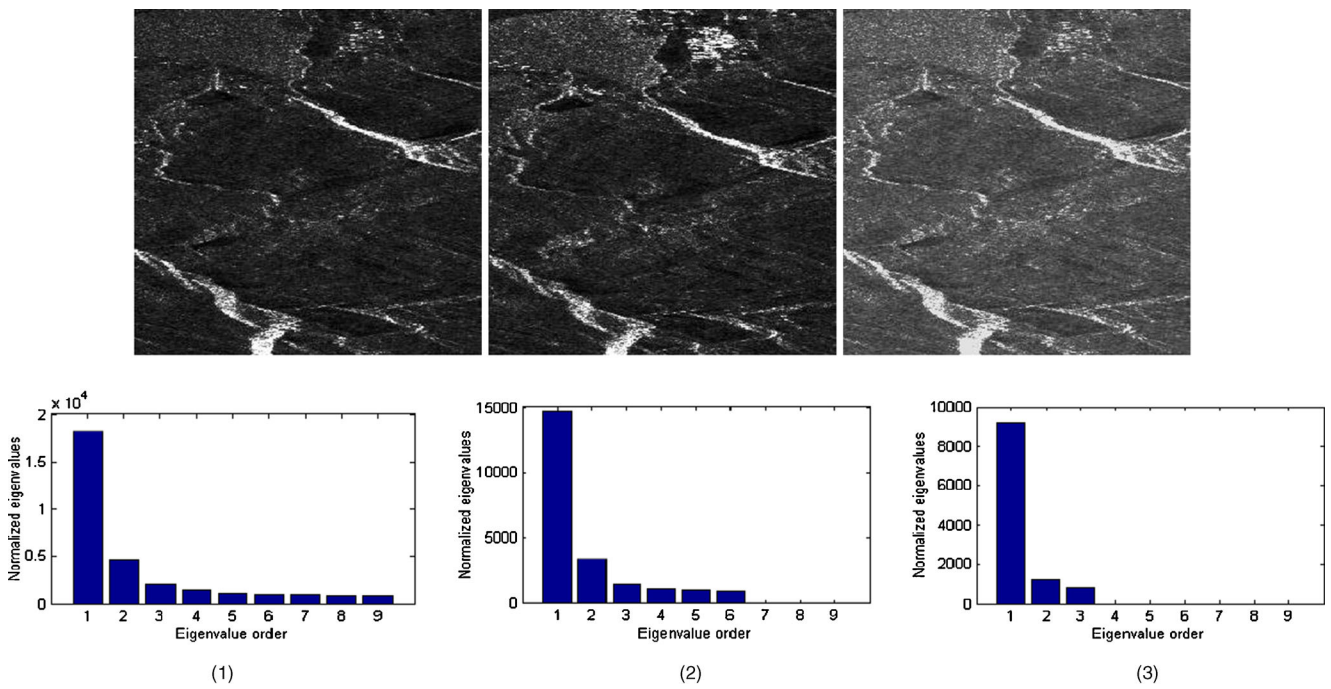
Fig. 2 Results of Fast ICA algorithms, and related eigenvalues for (*1*) one input (HV), (*2*) two inputs (HV and HH), and (*3*) three inputs (HV, HH, and VV), respectively

Gaussian). In this case, regarding the second characteristics arises from the ICA, a better separation occurs between image signal and speckle. Since a Gaussian component is separated from the other non-Gaussian components.

Independent Validation of Method

In order to assess the performance of filters, equivalent number of looks (ENL) and peak signal to noise ratio (PSNR) were used. ENL is a measure to assess the ability of smoothing speckle in an image and expresses a filter quality to reduce the speckle. Higher ENL values indicate better speckle reduction (Huang et al. 2009). The ENL value is calculated with the following equation:

$$ENL = \frac{\mu}{\sigma} \tag{12}$$

Where μ and σ represent the mean and variance of intensity image, respectively.
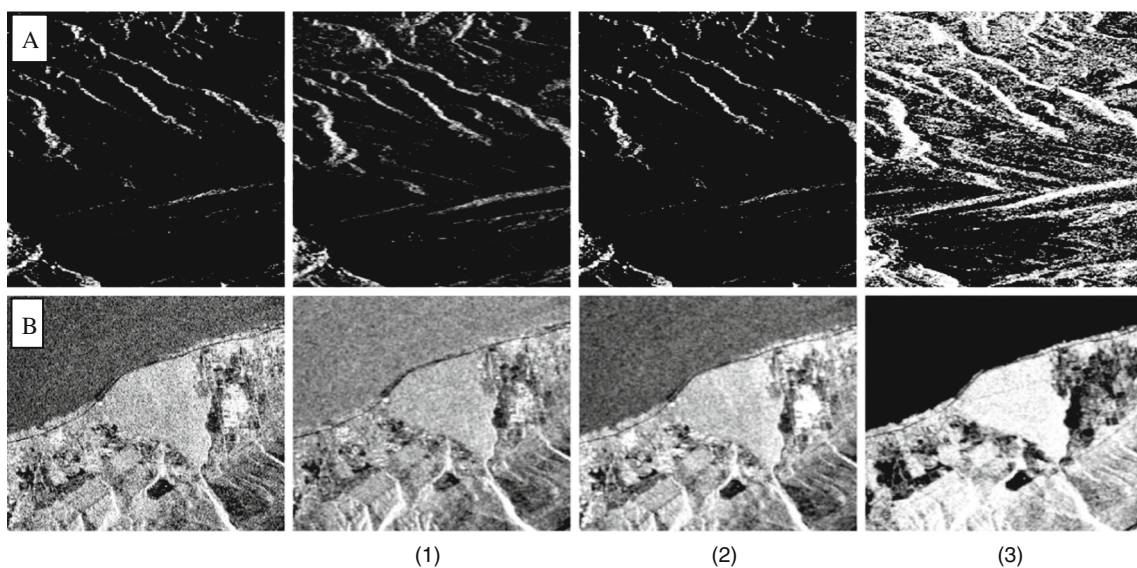

Fig. 3 The results of Fast ICA algorithms for the forest region in steep slopes of the terrain (**a**), and the forest region in the coast (**b**) for (*1*) one input (HV), (*2*) two inputs (HV and HH), and (*3*) three inputs (HV, HH, and VV). The first column is the original image

Table 1 ENL values for the forest region in steep slopes of the terrain (A), and the forest region in the coast (B)

Region type	Original image	One input (HV)	Two inputs (HV, HH)	ICA_HV, HH, VV
A	1.7	2.54	2.83	3.48
B	1.34	2.11	2.65	3.07

The PSNR equation is as follows:

$$PSNR = 10 \log_{10} \frac{(max(I))^2}{\frac{1}{NM}\sum_{i=1}^{N}\sum_{j=1}^{M}(y(i,j)-x(i,j))^2} \quad (13)$$

Where *max (I)* is Maximum intensity of unfiltered image, *M* and *N* are the numbers of image rows and columns, and *y(i, j)* and *x(i, j)* are the DN value of filtered image and the original image, respectively. Here, the difference should be measured with a reference image, which has the least value of speckle. Bigger PSNR values indicate better speckle reduction (Yu and Acton 2002).

Results and Discussion

In this section, the results of the speckle reduction using Fast ICA algorithm are presented. For this purpose, a part of the Fig. 1 with the dimensions of 300×300 pixels was used. In order to use the ICA algorithm a pre-processing is required and matrix must be converted to vector. In this case, we have a vector with the dimension of 90,000×1 for each image. A 90,000×3 matrix is generated and used as input of the ICA algorithm assuming three input images. In addition, the data matrix should be normalized in some cases. As mentioned in the previous section of the paper, the Fast ICA algorithm was used for simulation.

Figure 2 depicts ICA images with one input (HV), two input (HV and HH) and three inputs (HV, HH and VV) respectively. Speckle in the span image is somewhat better,

however texture of the image is affected. According to the calculated kurtosis, the ICA algorithm separates independent components based on the sorting of eigenvalues and orthogonalizing of the components. The speckle components have a random nature and contain small eigenvalues in the covariance matrix. On the other hand, signal components exist in several input images, as a consequence they are stronger and take larger eigenvalues.

As shown in Fig. 2, the eigenvalues of the target will be larger and the output image will represent more details when more input images are considered. As the number of inputs increased, fewer eigenvalues become larger and will have greater impact on the output image. Here, the first output of the ICA has been selected for display which is particularly caused by the largest amount of data set and most information is concentrated there. The other outputs of the algorithm have good information as well. The output of the smallest eigenvalues contains very little information and is considered as the output of the speckle. In order to have better evaluation, two forest types were selected from the Fig. 1. The first was a forest region in steep slopes of the terrain (A), and the second was a forest region in the coast (B) which is shown in Fig. 3 with the results of the filters.

The results of the ENL criteria in Table 1 show the improvement in ICA performance commensurate with increasing input numbers for both A and B regions. As can be seen, the ENL values in region A are 3.48, 2.83, and 1.7 for three, two, and one input images, respectively. The results in the region B are similar to region A but ENL values are lower than it. It should be noted that the original ENL has reached the maximum value in the input images. For example, in the region B, the maximum ENL value dedicated to HV channel.

In order to evaluate the performance of ICA algorithms, the number of inputs has increased in the next approach and some speckles with different variances has been added to polarimetric image in Fig. 2. For this purpose, the ICA output image with three inputs is considered as a reference image because of highest ENL and the PSNR is measured compared to this image. Full results of the PSNR and ENL for different number of inputs to ICA algorithm is presented in Table 2. The PSNR and ENL values for different speckle variances rise with increasing the number of inputs.

Table 2 The results of ENL and PSNR after adding virtual speckles with different variances

No. of inputs	$\sigma=0.001$		$\sigma=0.01$		$\sigma=0.1$		$\sigma=0.5$		$\sigma=1$		$\sigma=2$	
	ENL	PSNR	ENL	PSNR	ENL	PSNR	ENL	PSNR	ENL	PSNR	ENL	PSNR
One input (HV)	1.12	18.43	1.13	18.47	1.10	18.22	0.94	16.94	0.89	16.10	0.88	15.32
Two inputs (HV, HH)	1.63	25.41	1.46	25.42	1.46	24.43	1.50	21.33	1.46	19.97	1.50	18.79
Three inputs (HV, HH, VV)	1.83	50.82	1.85	40.49	1.85	30.59	1.74	23.81	1.73	22.08	1.80	20.87

Conclusion

Fast ICA method is not only efficient in reducing the speckle and keeping the details, but also it is very fast. ICA can process all of channels together that it could be helpful in avoiding from correlation between them. Removing the small eigenvalues in the calculation of ICA can reduce the information volume and on the other hand can significantly increase the processing speed. ICA algorithm has a great ability to separate signal from speckle. In order to increase the efficiency of ICA algorithm for separating signal from speckle the input data set to the algorithm can be increased. Various regions in ALOS PALSAR data was used in order to simulate the algorithms. This study has demonstrated that the topography of the area and forest density were also effective in this circumstance. In such a way that the kurtosis of the area's with forest coverage that are placed in areas with extreme topography such as mountains, are becoming close to ENL value equal to three earlier than those forest that are located in the flat areas such as beach hence the low power of the scatterer in the forests located in flat areas in compare to forests which are placed in mountains can be mentioned as the main reason. Using Fast ICA with large inputs number, in addition to processing speed and good separation of signal from noise, decrease the volume by removing the images with low eigenvalues.

References

Achim, A., Tsakalides, P., & Bezerianos, A. (2003). SAR image denoising via bayesian wavelet shrinkage based on heavy-tailed modeling. *IEEE Transactions on Geoscience and Remote Sensing, 41*(8), 1773–1784. doi:10.1109/TGRS.2003.813488.

Amini, J., & Sumantyo, J. T. S. (2009). Employing a method on SAR and optical images for forest biomass estimation. *IEEE Transactions on Geoscience and Remote Sensing, 47*(12), 4020–4026. doi:10.1109/TGRS.2009.2034464.

Anticoa, A. (2012). Independent component analysis of MODIS-NDVI data in a large South American wetland. *Remote Sensing Letters, 3*(5), 383–392. doi:10.1080/01431161.2011.603376.

Arsenault, H. H., & April, G. (1976). Properties of speckle integrated with a finite aperture and logarithmically transformed. *Journal of the Optical Society of America, 66*(11), 1160–1163. doi:10.1364/JOSA.66.001160.

Ballatorea, P. (2011). Extracting digital elevation models from SAR data through independent component analysis. *International Journal of Remote Sensing, 32*(13), 3807–3817. doi:10.1080/01431161003777213.

Chenab, F., Guanc, Z., Yangab, X., & Cuia, W. (2011). A novel remote sensing image fusion method based on independent component analysis. *International Journal of Remote Sensing, 32*(10), 1649–1663. doi:10.1080/01431161003743207.

Cheng, X., Huangb, W., & Gonga, J. (2013). A decomposition-free scattering mechanism classification method for PolSAR images with Neumann's model. *Remote Sensing Letters, 4*(12), 1176–1184. doi:10.1080/2150704X.2013.858840.

Chitroub, S., & Hachemi, R. (2007). "Independent component analysis of POLSAR images. Relative newton-based approach," Paper presented at the IEEE International Conference on Signal Processing and Communications, Dubai, November 24–27.

Dabboora, M., Yackelb, J., Hossainb, M., & Braunc, A. (2013). Comparing matrix distance measures for unsupervised POLSAR data classification of sea ice based on agglomerative clustering. *International Journal of Remote Sensing, 34*(4), 1492–1505. doi:10.1080/01431161.2012.727040.

Frost, V. S., Stiles, J. A., Shanmugan, K. S., & Holtzman, J. C. (1982). A model for radar images and its application to adaptive digital filtering of multiplicative noise. *IEEE Transactions Pattern on Analysis and Machine Intelligence, 4*(2), 157–166. doi:10.1109/TPAMI.1982.4767223.

Gao, G. (2010). Statistical modeling of SAR images: a survey. *Sensors, 10*(1), 775–795. doi:10.3390/s100100775.

Gonzalez, A. A., Martinez, C. L., & Salembier, P. (2012). Filtering and segmentation of polarimetric SAR data based on binary partion trees. *IEEE Transactions on Geoscience and Remote Sensing, 50*(2), 593–605. doi:10.1109/TGRS.2011.2160647.

Huang, S. Q., Liu, D. Z., Gao, G. Q., & Guo, X. J. (2009). A novel method for speckle noise reduction and ship target detection in SAR images. *Journal of Pattern Recognition, 42*(7), 1533–1542. doi:10.1016/j.patcog.2009.01.013.

Kharbouchea, S., & Claveta, D. (2013). Speckle reducing in PolSAR images for topographic feature extraction. *International Journal of Image and Data Fusion, 4*(2), 146–158. doi:10.1080/19479832.2012.710270.

Kuan, D. T., Sawchuk, A. A., Strand, T. C., & Chavel, P. (1985). Adaptive noise smoothing filter for images with signal-dependent noise. *IEEE Transactions on Pattern Analysis and Machine Intelligence, 7*(2), 165–177. doi:10.1109/TPAMI.1985.4767641.

Kuan, D. T., Sawchuk, A. A., Strand, T. C., & Chavel, P. (1987). Adaptive restoration of images with speckle. *IEEE Transactions on Acoustics, Speech, and Signal Processing, 35*(3), 373–383. doi:10.1109/TASSP.1987.1165131.

Lee, J. S. (1980). Digital image enhancement and noise filtering by use of local statistics. *IEEE Transactions on Pattern Analysis and Machine Intelligence, 2*(2), 165–168. doi:10.1109/TPAMI.1980.4766994.

Lee, J. S., & Hoppel, K. (1992). Principal components transformation of multifrequency polarimetric SAR imagery. *IEEE Transactions on Geoscience and Remote Sensing, 30*(4), 686–696. doi:10.1109/36.158862.

Lee, J. S., & Pottuier, E. (2009). *Polarimetric Radar Imaging: from basics to applications* (1st ed.). USA: CRC press.

Lee, J. S., Grunes, M. R., & Mango, S. A. (1991). Speckle reduction in multipolarization, multifrequency SAR imagery. *IEEE Transactions on Geoscience and Remote Sensing, 29*(4), 535–544. doi:10.1109/36.135815.

Li, H., Huang, B., & Huang, X. (2010). A level set filter for speckle reduction in SAR images. *EURASIP Journal on Advances in Signal Processing, 2*(1), 1–14. doi:10.1155/2010/745129.

Lopes, A., Touzi, R., & Nezry, E. (1990). Adaptive speckle filters and scene heterogeneity. *IEEE Transactions on Geoscience and Remote Sensing, 28*(6), 92–100. doi:10.1109/36.62623.

Lopez-Martinez, C., & Fabregas, X. (2003). Polarimetric SAR speckle noise model. *IEEE Transaction on Geoscience and Remote Sensing, 41*(10), 2232–2242. doi:10.1109/TGRS.2003.815240.

Solbo, S., & Eltoft, T. (2002). A stationary wavelet-domain wiener filter for correlated speckle. *IEEE Transactions on Geoscience and Remote Sensing, 46*(4), 1219–1230. doi:10.1109/TGRS.2007.912718.

Wang, H. (2009). "Comparison of two ICA based methods for speckle reduction of polarimetric SAR images." Paper presented at the IEEE

Asia-Pacific Conference on Information Processing, Shenzhen, July 18–19.

Wang, H., Pi, Y., Liu, G., & Chen, H. (2008). Applications of ICA for the enhancement and classification of Polarimetric SAR images. *International Journal of Remote Sensing, 29*(6), 1649–1663. doi: 10.1080/01431160701395211.

Xinga, X., Jia, K., Zoua, H., & Suna, J. (2013). Feature selection and weighted SVM classifier-based ship detection in PolSAR imagery. *International Journal of Remote Sensing, 34*(22), 7925–7944. doi: 10.1080/01431161.2013.827812.

Yu, Y., & Acton, S. T. (2002). Speckle reducing anisotropic diffusion. *IEEE Transactions on Image Processing, 11*(11), 1260–1270. doi: 10.1109/TIP.2002.804276.

Yusheng, F., Xiaoning, C., Yiming, P., & Yinming, H. (2005). The fast fixed-point algorithm for speckle reduction of polarimetric SAR image. *Journal of Electronics, 22*(3), 288–293. doi:10.1007/BF02687985.

Zhanga, L., Zoua, B., Haob, H., & Zhanga, Y. (2011). A novel super-resolution method of PolSAR images based on target decomposition and polarimetric spatial correlation. *International Journal of Remote Sensing, 32*(17), 4893–4913. doi:10.1080/01431161.2010.492251.